FISEVIER

Contents lists available at ScienceDirect

## Materials Chemistry and Physics

journal homepage: www.elsevier.com/locate/matchemphys



# Understanding thermodynamic stability and carbothermal reduction in SiOC

Rahul Ananda, Kathy Lua, b, \*

- a Department of Materials Science and Engineering, 260 Holden Hall, Virginia Polytechnic Institute and State University, Blacksburg, VA, 24061, USA
- b Department of Mechanical and Materials Engineering, EEC Building 257, University of Alabama at Birmingham, AL, 35294, USA

#### ARTICLE INFO

Keywords:
Silicon oxycarbide
Phase
Atomic structure
Gibbs free energy
Carbothermal reduction

#### ABSTRACT

This study explores the phase evolution, carbothermal reduction, and energetics in SiO  $_{\rm C}$  derived from the pyrolysis of trimethylsilyl terminated polyhydromethylsiloxane (PHMS-TMS) from 1200 to 1600 °C. High-resolution X-ray photoelectron spectroscopy (XPS) shows notable differences in the constituent bond arrangement between the more Si-rich SiOC ceramics and the more C-rich SiOC ceramics, which subsequently affects the microstructure of the SiOC systems. Carbothermal reduction starts at lower temperatures than previously reported and indicates no phase separation of SiOC or formation of SiO $_{\rm C}$  nanodomains. The thermodynamic stability of the thus-obtained SiOC ceramics is evaluated using a Gibbs free energy minimization method. The results suggest that differences in silicon mixed bonding environments and their relative amounts (SiO $_{\rm C}$  $_{\rm C}$ , SiOC $_{\rm S}$ , or SiC $_{\rm A}$ ) lead to differences in thermodynamic stability.

## 1. Introduction

Silicon oxycarbide, which is an amorphous single-phase ceramic of empirical formula SiO  $_{\rm C}$  , is composed of nanodomains of SiO  $_{\rm 2}$ , graphene-like C sheets, and mixed bond tetrahedra of Si–O/C [1–4]. At high pyrolysis temperatures, it is generally accepted that the SiO  $_{\rm 2}$  phase reacts with the free carbon present to form SiC [5,6], which is the primary mechanism for SiC formation in polymer-derived ceramics [4]. At temperatures greater than 1300 °C, there is a notable decrease in O composition paired with the formation of  $\beta$ -SiC [7–9]. This is the well-accepted carbothermal reduction of Si–O bonds by C=C/C–C and the formation of SiC through Si–C bonds. However, the specific process involved in the SiOC conversion to SiC and the roles of O and C are still not understood [10].

Carbothermal reduction is characterized by two aspects: the reduction of  $SiO_2$  and the formation of  $\beta$ -SiC. There have been many theorized reaction routes (Eqs. (1)–(5)) that lead to the reduction of  $SiO_2$ . Eq. (1) forms a SiO gas intermediate and Eqs. (2-5) create SiC [1,6–8,11].

$$SiO_{g}(s) + C(s) \rightarrow SiO(g) + CO(g)$$
 (1)

$$SiO(g) + 2C(s) \rightarrow SiC(s) + CO(g)$$
 (2)

$$2SiO(g) + 3C(s) \rightarrow 2SiC(s) + CO2(g)$$
 (3)

$$Si(s) + CO(g) \rightarrow SiC(s) + 1/2O_{2}(g)$$
(4)

$$Si(s, l, g) + C(s) \rightarrow SiC(s)$$
 (5)

Further, a few studies claim the formation of SiC as a result of the interactions between the intermediate SiO $_{v}$ C $_{d,v}$  fractions [12]:

$$SiO_2C_2 + SiO_2C_2 \rightarrow SiC_4 + SiO_4$$
 (6)

$$SiO_{2}C_{2} + SiO_{3}C \rightarrow SiOC_{3} + SiO_{4}$$
 (7)

$$SiOC_{3} + SiO_{3}C \rightarrow SiC_{4} + SiO_{4}$$
(8)

The above reported processes assume that  $SiO_2$  and free C react and O leaves the system as CO [7,8]. However, there is no evidence that SiOC converts to  $SiO_2$  or Si nanodomains first and then reacts with free C to form SiC. Furthermore, use of dopants (e.g., Ti) can accelerate the formation of SiC in SiOC systems at lower temperatures without the formation of  $SiO_4$  structural units [13].

The current work aims to understand the carbothermal reduction process of the SiO  $_{\rm C}^{\rm C}_{\rm b}$  matrix at  $\geq 1200$  °C with the formation of stoichiometric SiO  $_{\rm C}^{\rm C}_{\rm b}$  using a more Si-rich PHMS-TMS precursor with low or no free carbon phases. The energetics of these SiO  $_{\rm C}^{\rm C}_{\rm b}$  systems was studied and their thermodynamic stability was analyzed by a Gibbs free energy minimization method.

E-mail address: klu@uab.edu (K. Lu).

https://doi.org/10.1016/j.matchemphys.2024.129123

Received 13 December 2023; Received in revised form 11 February 2024; Accepted 21 February 2024 0254-0584/© 20XX

<sup>\*</sup> Corresponding author. Department of Materials Science and Engineering, 260 Holden Hall, Virginia Polytechnic Institute and State University, Blacksburg, VA, 24061, USA.

## 2. Experimental procedure

A trimethylsilyl terminated PHMS (Fig. 1, PHMS-TMS, MW = 1400-1800 g/mol, HMS-993, Gelest Inc., USA) was used as the precursor. It is a comparatively carbon-deprived (20.00 wt% C in the monomer) transparent liquid at room temperature and a commonly used precursor to produce more Si-rich SiOC ceramics.

The PHMS precursor was mixed with 0.05 wt% Karstedt's catalyst (2.1–2.4 wt% platinum–divinyltetramethyldisiloxane in xylene, Millipore Sigma) in an ambient atmosphere for 30 min and stirred with a magnetic stirrer at room temperature. The mixed solution was transferred into an aluminium pan and kept at 80 °C for 48 h for gelation. Then the aluminium pan with the precursor was heated to 120 °C for 24 h to obtain a transparent monolith solid precursor. The resulting sample was further shaped into pellets through a gel-cutting tool. Afterwards, the gel-cast samples were transferred to a vacuum oven for crosslinking at 250 °C for 2 h at a heating rate of 2 °C/min. The crosslinking of the samples was facilitated by the condensation reaction due to air/moisture, and the hydrosilylation reaction initiated by the vinyl and phenyl bonds present in the catalyst was responsible for the crosslinking reaction. The detailed mechanism of the crosslinking for pure PHMS samples was studied in previous work [14].

The crosslinked pellets were pyrolyzed at temperatures ranging from 1200 °C to 1600 °C for 2 h in an alumina tube furnace (Inner diameter 55 mm, Horizontal Tube Furnace, CM Furnaces Inc., Bloomfield, NJ, USA) under an argon atmosphere (Industrial grade Ar. 99.99% purity, Airgas, Christiansburg, VA, USA). The selection of the temperature range for this study was based on the combination of scientific understanding need and relevance to potential applications. The currently chosen precursor converts to SiOC in the range of 700-800 °C. The obtained amorphous SiOC remains in an amorphous phase below 1100 °C but crystalizes (due to the rearrangement of the fractals,  $SiO_{v}C_{4.v}$ , x = 0-4) on further pyrolysis. Typically, the carbothermal reduction process starts above 1200 °C and SiOC converts to SiC at higher pyrolysis temperatures. The rearrangement of the SiOC fractal structure and the carbothermal reduction process involve molecular arrangement, phase evolution, and mass loss. Thus, the analysis of the structural stability of SiOC from 1200 °C to 1600 °C is extremely important. The temperature ramp rate and gas flow rate were maintained at 2 °C/ min and 300 ml/min during the entire heating and cooling process, respectively. The samples were named as PHMS-XX00. In the sample codes, e.g., in PHMS-1200, '1200' indicates the pyrolysis temperature of the sample in Celsius.

The pyrolyzed samples were milled with a sillimanite agate mortar and the phases were identified by X-ray diffraction (Bruker XRD D8, MA, USA) with Cu K $\alpha$  radiation ( $\lambda = 1.5408$  Å) in the 2 $\theta$  range of  $10^{\circ}$ – $80^{\circ}$  with a uniform scan rate of  $3^{\circ}$  min<sup>-1</sup> and a step size of  $0.05^{\circ}$ . The peaks were identified with reference to a crystal structure database (ICDD). Polynomial fitting of the XRD curves per the Gaussian function was performed to calculate the full width at half-maximum (FWHM) of the maximum  $\beta$ -SiC peak intensity. The crystallite sizes of the phase separated  $\beta$ -SiC were calculated using the Scherrer formula. We carried out a series of studies using Fourier transform infrared spectroscopy, thermogravimetric analysis [15–19], high energy XRD [20], Reactive

$$CH_3$$
 $H_3C$ 
 $CH_3$ 
 $CH_3$ 
 $CH_3$ 
 $CH_3$ 
 $CH_3$ 
 $CH_3$ 
 $CH_3$ 
 $CH_3$ 
 $CH_3$ 
 $CH_3$ 

Fig. 1. Molecular structure of the PHMS-TMS precursor.

Force Field simulation [10,21], and 4D scanning transmission electron microscopy [22]. Those studies, though insightful, did not provide additional insight. Thus, in this study, the chemical compositions and structures were detected by X-ray photoelectron spectroscopy (XPS, PHI Quantera SXM-03, Kanagawa, Japan) using an Al Kα X-ray (1486.7 eV) source with an analyzed area of about 200  $\mu m$  in diameter. The fractured surface of the samples was placed at an electron take-off angle of 55°. Multiple survey scans at different locations of the samples and the corresponding high-resolution peaks were obtained after Ar ion milling in order to obtain the most accurate elemental compositions and bonds. An electron flow of 20 µA was applied to the samples to counter the electrostatic charge. High resolution peaks were fitted by PHI MultiPak software. Further, the microstructure images were recorded using scanning electron microscopy (SEM, JSM IT-500HR, JEOL, Tokyo, Japan) at an accelerating voltage of 20 kV. The SEM images illustrated morphological and structural changes of the SiO C, samples at different pyrolysis temperatures.

## 3. Results and discussion

#### 3.1. Phase evolution

The structural evolution of the SiOC ceramics derived from the PHMS-TMS precursor is shown in Fig. 2. The SiOC ceramic pyrolyzed at 1200 °C (PHMS-1200) exhibits an amorphous structure. There is no broad hump at ~22° 2 $\theta$  angle. This can be ascribed to the absence of SiO<sub>2</sub> nanodomains in the SiOC ceramic matrix [23]. The diffraction pattern of the PHMS-1400 sample exhibits a pseudo-amorphous structure. The small hump at  $2\theta = 35.8^{\circ}$ , albeit weak, is indicative of the forma-

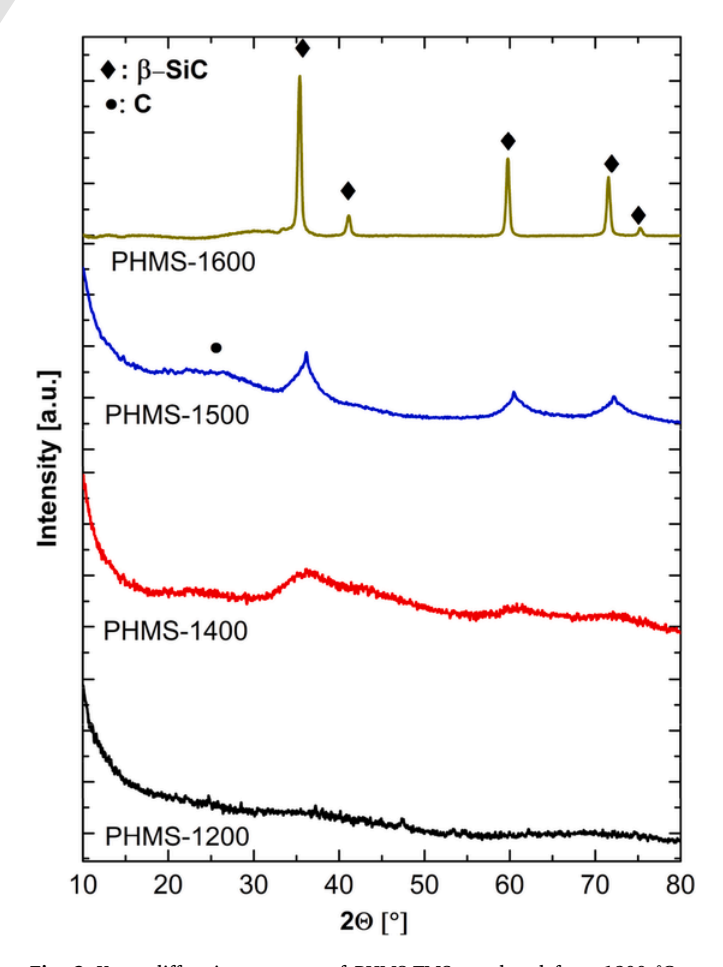


Fig. 2. X-ray diffraction patterns of PHMS-TMS pyrolyzed from 1200  $^{\circ}\text{C}$  to 1600  $^{\circ}\text{C}$  in argon.

tion of SiC nuclei due to Si–O–C bond rearrangement in the SiOC matrix

The SiOC ceramic pyrolyzed at 1500 °C is pseudo-amorphous with a weak peak at 26.2° 20 angle, representing the C phase (ICDD-00-075-1621) in the SiOC matrix. The presence of merely discernible peaks of  $\beta\text{-SiC}$  (ICDD-01-073-1665) indicates that  $\beta\text{-SiC}$  is embedded in the amorphous SiOC matrix along with fine crystallites of free C. Further pyrolysis of the PHMS-TMS precursor at 1600 °C converts the SiOC ceramic matrix into  $\beta\text{-SiC}$ . The average crystallite size of SiC has been calculated using the most intense peak of the crystallites. After 1500 °C and 1600 °C pyrolysis, the sizes of SiC nucleated and phase separated from the SiOC matrix are 3.1 and 18.6 nm, respectively. Also, the drastic increase in the size of crystalline SiC in SiOC demonstrates phase separation, crystallization, and decomposition of the SiOC matrix, which involves the carbothermal reduction of different Si–O and Si–C bonds present in the SiOC systems.

#### 3.2. Atomic bonding change

The XPS survey patterns of PHMS-1200, PHMS-1400, PHMS-1500, and PHMS-1600 are given in Fig. 3. Fig. 3a shows the presence of O1s, C1s, Si2s, and Si2p peaks for all the samples. The corresponding atomic concentrations of the respective elements are shown in Table 1, which indicates that PHMS-1500 has the highest Si concentration. The free C present in the SiOC system was calculated as described in previous literature [24–27]. PHMS-1500 shows a C/Si ratio at  $\sim\!0.6$  and has no free C. PHMS-1600 has a C/Si ratio of  $\sim\!1$  and a small amount of free C. Also, the concentration of O (O/Si) consistently decreases as the pyrolysis temperature increases.

Deconvolution of the Si2p spectra (Fig. 3b) of PHMS-1200 and PHMS-1400 yields three peaks at  $\sim$ 101.8,  $\sim$ 101, and  $\sim$ 100 eV, corresponding to the SiO<sub>2</sub>C<sub>2</sub>, SiOC<sub>3</sub>, and SiC<sub>4</sub> phases, respectively [28]. There is a gradual right shift of the Si2p spectra for the pyrolyzed PHMS samples. The Si2p peak at  $\sim$ 98.5 eV indicates the Si–Si<sub>4</sub> peak in the PHMS-1600 sample [29].

The content of the SiC, phase calculated from the peak area increases from 17.8% to 79.3%. The content of Si-Si, calculated from the peak area ratio is 8.5%. There is no evidence of SiO<sub>4</sub> and SiO<sub>5</sub>C phases in the SiOC samples. On the contrary, elemental "Si" is observed in the SiOC matrix at higher pyrolysis temperatures. The exact state of Si can be understood as follows. The amorphous Si peak generally shows a broad hump at  $\sim 28.4^{\circ}$  of 20, which is absent in the diffraction pattern of SiOC at 1600 °C (Fig. 2). Also, Si cannot remain in an amorphous state at such a high temperature (~1600 °C). However, the Si peak area ratio with SiC is significant enough in the XPS plot (Fig. 3), implying that a reasonable amount of Si is present in the SiOC system. This suggests that Si is neither in the amorphous state nor in the phase separated state (elemental Si). Thus, we conclude that the "Si" present here is not phase-separated from the backbone of the Si-O-C units, rather it remains as  $C_4$ -Si/Si-Si $_4$  mixed bond in the Si $_m$ C $_n$  network (since there are no Si diffraction peaks in the XRD results). Regardless, there is no evidence of SiO<sub>2</sub> phase present at any pyrolysis temperature. This contradicts the generally accepted carbothermal reduction understanding in the more Si rich-SiOC systems (Eqs. (1)-(5)) [1,6-8,11]. Previous studies reported that with temperature increase, both SiC, and SiO, units increase [30-32]. However, for the current system, there is no SiO cluster present. Also, the O-containing unit fractions decrease in the PHMSderived SiOC system. This is supported by the XRD results (Fig. 2) in that the hump at  $22^{\circ}$  of  $2\theta$ , which is due to the presence of tetrahedral Si–O/Si–C units in  $SiO_aC_b$ , shifts towards right with the increase of pyrolysis temperature.

Fig. 3c shows the high resolution XPS C1s peaks of the pyrolyzed PHMS samples. Si–C, C = C, and C - C bonds in SiOC are at ~281.5, ~282.6, and ~284.7 eV, respectively. The C1s peak gradually shifts towards the lower binding energy with increase in the pyrolysis tem-

perature. This indicates a transition from a more electronegative environment to a less electronegative one, i.e., O-containing bonds with Si decrease in the SiO  $_{\rm C}$  matrix with pyrolysis temperature increase. Also, a decrease in C=C bonds with pyrolysis temperature increase (Fig. 3c) and O from the SiO  $_{\rm C}$  system indicate their removal, most likely in the form of CO/CO $_{\rm 2}$ . The PHMS-1500 and PHMS-1600 samples contain mainly Si–C (of SiC $_{\rm 4}$  units) and C=C bonds (residual carbon).

Fig. 3d shows the O1s peaks of the sample spectra. The correspondingly deconvoluted spectra exhibit the presence of Si–O and C=O bonds at  $\sim\!530.7$  eV, and  $\sim\!531.5$  eV binding energy, respectively. A shift to lower binding energy suggests that the oxygen atoms are experiencing a decrease in the attractive force from the nucleus, which can be associated with electron donation or a decrease in the electron attraction nature of neighbouring Si atoms. Thus, the O1s peak shift towards lower binding energy demonstrates the removal of O-containing Si bonds with pyrolysis temperature increase. The C–O bonds may correspond to bond signatures from foreign oxygen/CO $_2$  absorbed on the sample surface as reported previously [28,33]. Fig. 4 shows the model for structural evolution during the carbothermal reduction of the SiOC system in this study.

Overall, the XPS spectra show the formation of Si–C bonds and the elimination of C–O and Si–O bonds with increase in pyrolysis temperature. For the Si–O and C–O bonds, the intensity of the C–O bonds decreases rapidly, indicating the release of  ${\rm CO/CO}_2$  from the SiOC structure during the carbothermal reduction of SiOC. Further, there is no evidence of Si–O bond increase or formation of SiO $_4$  units in the structure, implying the absence of segregation and clustering of O-rich and C-rich SiC  $_4$  units in the SiOC network. Therefore, the formation of SiC or transformation of SiO $_4$  to SiC is not driven by the phase separation or formation of SiO $_4$  clusters or SiO $_2$  nanodomains. Rather, it depends on the thermodynamical stability of Si–O, C–O, and Si–C bonds or intermediate SiO  $_4$  fractions present in the system.

## 3.3. Thermodynamic stability

From a different perspective, energetics of a Si-rich PHMS-TMS derived SiOC phase can provide an important understanding to their thermodynamic stability at high temperatures. Since the H content in the SiOC is negligible for samples pyrolyzed at 1000 °C and above [34], the SiO $_{\rm a}{\rm C}_{\rm b}$  compositions from the XPS results can be used for the thermodynamic calculation [35]. Here, we consider the thermodynamic stability of the SiOC relative to a mixture of probable nanodomains of SiC, SiO $_{\rm 2}$ , and C $_{\rm free}$  (Eq. (2)) in order to calculate the intermediate phase fractions present in the SiO $_{\rm a}{\rm C}_{\rm b}$  system. The Gibbs free energy of formation,  $^{\Delta G}\!_f$ , is generally written as:

$$\Delta G_f(T) = \Delta H_f(T) - T \Delta S_f(T)$$
 (10)

Where  $\Delta S$  is the entropy of formation.  $\Delta S_f$  can be calculated by the following equation [36,37]:

$$\Delta S_f = -R \sum_{i=0}^{4} f_i(T) \ln(f_i(T)) \tag{11}$$

Here,  $f_i$  (T) (i = 0–4) is the fractions of SiO $_x$ C $_y$  as SiO $_{(4-i)/2}$ C $_{i/4}$  domains and R is the gas constant.  $f_i$  (T) has been computed by using the Gibbs free energy minimization code through Mathematica software as described previously (also provided in the supplement) [9,27,38]. The overall Gibbs free energy of the amorphous SiO $_x$ C $_y$  system can be represented as:

$$\Delta G_f = \sum_{i=0}^{4} f_i(T) \cdot G_i(T) + RT \sum_{i=0}^{4} f_i(T) \cdot \log f_i(T)$$
 (12)

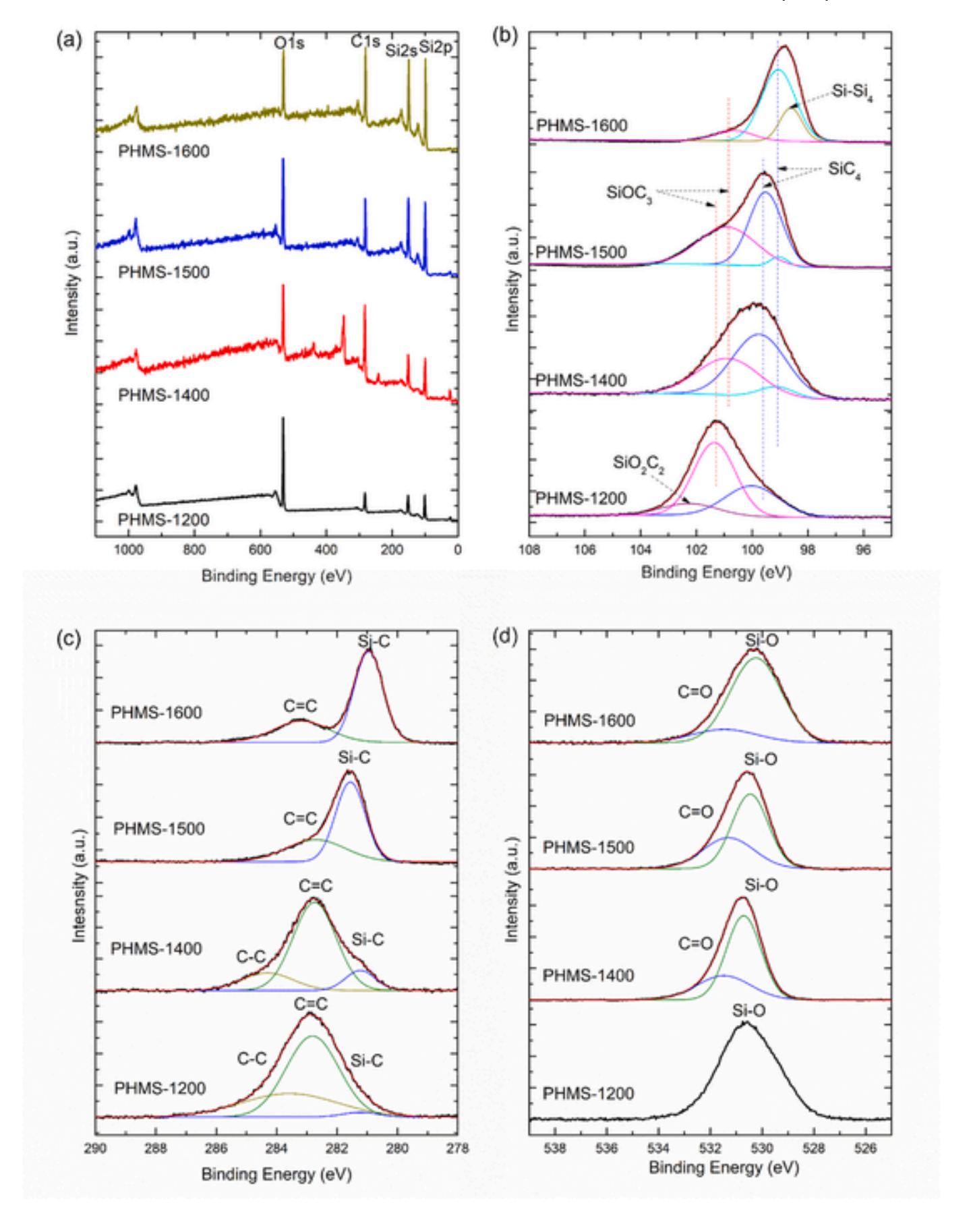


Fig. 3. (a) XPS survey spectra of the PHMS-TMS derived SiOC samples pyrolyzed at 1200 °C–1600 °C. The corresponding high-resolution spectra of (b) Si2p, (c) C1s, and (d) O1s.

Table 1
Elemental compositions of the SiOC samples at different pyrolysis temperatures

| Samples   | Elemen | t Content | (at%) | Empirical formula  | C/Si | O/Si |
|-----------|--------|-----------|-------|--|------|------|
|           | Si     | О         | С     |  |      |      |
| PHMS-1200 | 24.42  | 46.09     | 29.49 | $SiO_{1.88}^{}C_{0.06}^{} + 1.15C_{free}^{}$             | 1.21 | 1.89 |
| PHMS-1400 | 23.3   | 23.69     | 52.99 | $SiO_{1.02}^{1.88}C_{0.49}^{0.00} + 0.53C_{free}^{1.88}$ | 2.27 | 1.02 |
| PHMS-1500 | 41.05  | 34.22     | 24.73 | SiO C 0.49   | 0.60 | 0.83 |
| PHMS-1600 | 39.73  | 22.18     | 38.09 | $SiO_{0.56}^{0.6}C_{0.72}^{0.0} + 0.24C_{free}$          | 0.96 | 0.56 |

The Gibbs free energy of formation and thus  $f_i$  (T) obtained are listed in Table 2. The configurational entropy value for PHMS-1400 is the highest among all the SiO C compositions obtained after pyrolysis. Further, the calculated "T  $\Delta S_{j}^{r,\nu}$ " at 1400 °C shows the highest negative

value for PHMS-1400 and confirms the corresponding SiOC thermodynamic stability (at 1400 °C) with respect to crystallization. The enthalpy of formation for the SiOC systems becomes less exothermic, and the Gibbs free energy of formation continuously increases with the increase in pyrolysis temperature. Therefore, PHMS-1200 and PHMS-1400 are thermodynamically more stable compared to PHMS-1500 and PHMS-1600.

## 3.4. Microstructure evolution

The ceramics obtained after pyrolysis at different temperatures are glassy and brittle (Fig. 5). The micrographs of PMHS-1200 (Fig. 5a), PHMS-1400 (Fig. 5b), and PHMS-1500 (Fig. 5c) show that the samples are dense. However, at 1500 °C (Fig. 5c), uniform nanopores with random nano-cracks can be observed. Furthermore, the SEM image of

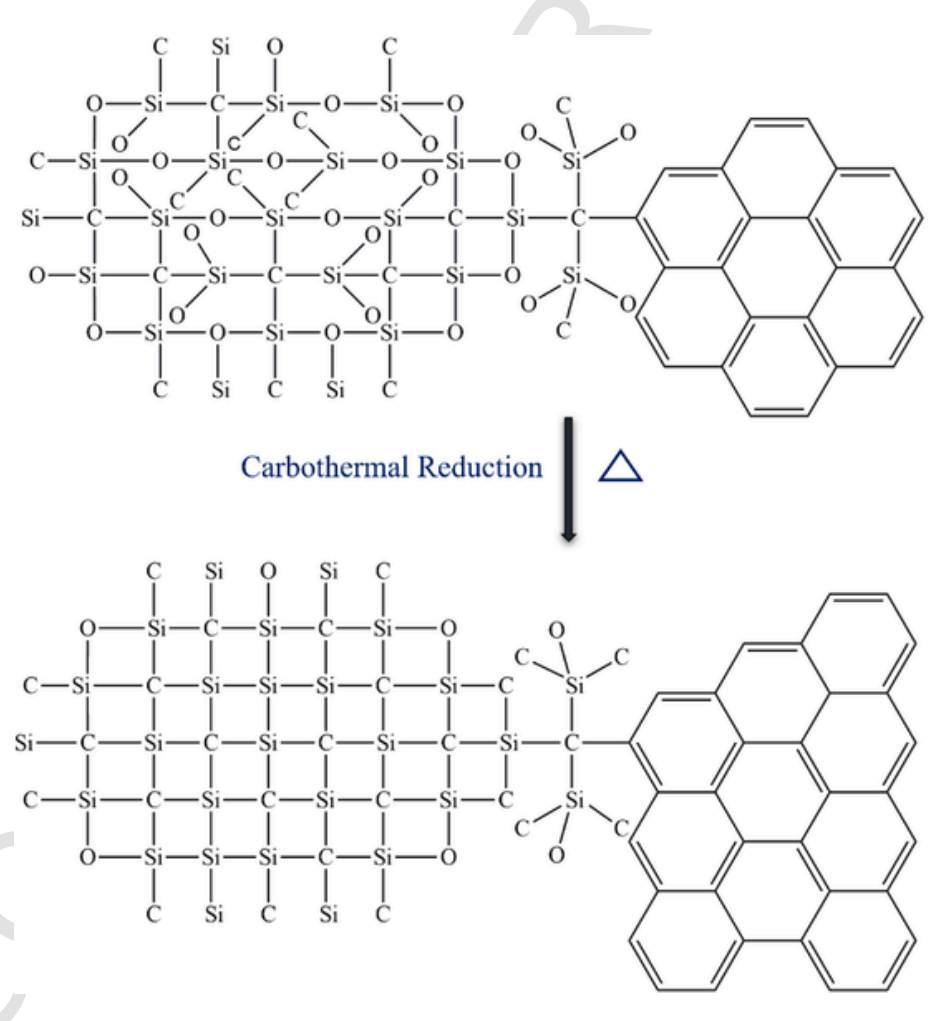


Fig. 4. Illustration of structural changes in SiOC during conversion of SiOC to SiC.

**Table 2** Fractions ( $f_i$ ) (i = 0–4) of component SiO<sub>(4-i)/2</sub>C<sub>i/4</sub> of the SiOC domains (SiO<sub>x</sub>C<sub>y</sub>) used for estimating the configurational entropies  $\Delta S_f$  and the entropy terms -T  $\Delta S_f$  of the SiOC samples.

| Samples   | $f_0$ | $f_1$ | $f_2$ | $f_3$ | $f_4$ | $\Delta G_f$ (kJ·K <sup>-1</sup> ·mol <sup>-1</sup> ) | $\Delta H_f$ (kJ·K <sup>-1</sup> ·mol <sup>-1</sup> ) | $\Delta S_f (J \cdot K^{-1} \cdot mol^{-1})$ | $-T$ $\Delta S_f$ (kJ·mol <sup>-1</sup> ) at 1400 °C |
|-----------|-------|-------|-------|-------|-------|---|---|--|--|
| PHMS-1200 | 0.79  | 0.13  | 0.05  | 0.02  | 0     | -327.10   | -318.78   | 1.35   | -9.45  |
| PHMS-1400 | 0.14  | 0.21  | 0.26  | 0.33  | 0.06  | -224.61   | -203.92   | 12.37  | -20.7  |
| PHMS-1500 | 0.07  | 0.14  | 0.24  | 0.43  | 0.12  | -196.02   | -175.10   | 11.81  | -19.77   |
| PHMS-1600 | 0.02  | 0.07  | 0.18  | 0.49  | 0.24  | -163.36   | -143.65   | 10.51  | -17.60   |

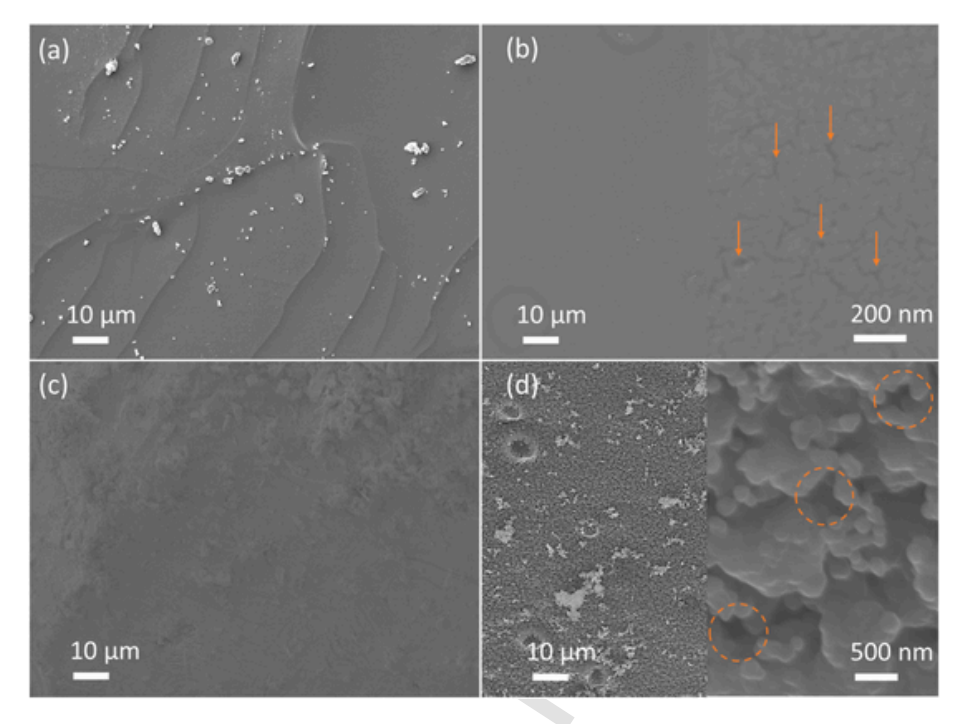


Fig. 5. SEM micrograph of PHMS-TMS pyrolyzed at (a) 1200 °C, (b) 1400 °C, (c) 1500 °C, and (d) 1600 °C. The right-hand sides of (b) and (d) are the corresponding high-resolution SEM images of the samples pyrolyzed at 1400 °C and 1600 °C, respectively.

PHMS-1600 (Fig. 5d) shows the presence of open pores. This porous structure of the sample is due to the phase separation as well as the carbothermal reduction of the SiOC sample to SiC at this pyrolysis temperature. The high-resolution SEM image of PHMS-1400 shows a uniform and crack-free microstructure (Fig. 5b), yet a few nanopores (shown with arrows) are observed. However, the high-resolution microstructure of PHMS-1600 (Fig. 5d) shows aggregated particles. Pores of 0.5–1  $\mu m$  (shown within the circles) can be seen throughout the micrographs. These pores or cracks are primarily due to phase separation and carbothermal reduction of SiOC ceramics. Predominantly, CO gas releases during carbothermal reduction along with CO $_2$  (as shown in Eqs. (1)–(3)).

### 4. Conclusions

This study explores the structural evolution of PHMS-TMS (a relatively Si-rich precursor) derived SiO $_a$ C $_b$  during pyrolysis. The SiOC obtained is of stoichiometric composition at 1500 °C. There is a deficiency of SiO $_a$  units among all possible mixed SiOC units. A crystalline  $\beta$ -SiC phase is observed at 1600 °C. The carbothermal reduction process (the conversion of SiOC to SiC) starts at lower temperatures and indicates no phase separation of SiOC or formation of SiO $_a$  (SiO $_a$  nanodomains). The carbothermal reduction process into the more Si-rich SiOC system is driven by the elimination of C–O bonds followed by S–O bonds and thus is a continuous process. Further, the carbothermal reduction process reduces the thermodynamic stability of SiO $_a$ C $_b$  ceramic. The thermodynamic stability of the PHMS-TMS derived SiO $_a$ C $_b$  is highest for pyrolysis temperatures below 1400 °C. Also, carbothermal reduction creates porous SiOC/SiC structures at pyrolysis temperatures above 1400 °C.

## **Funding information**

This work received financial support from the National Science Foundation under Grant No. CBET-2024546 and the Air Force Office of Scientific Research under grant number FA9550-22-1-0081.

#### CRediT authorship contribution statement

Rahul Anand: Writing – original draft, Visualization, Methodology, Investigation, Formal analysis, Data curation, Conceptualization. Kathy Lu: Writing – review & editing, Visualization, Validation, Supervision, Resources, Project administration, Funding acquisition, Formal analysis, Conceptualization.

### **Declaration of competing interest**

The authors declare the following financial interests/personal relationships which may be considered as potential competing interests: Kathy Lu reports financial support was provided by the National Science Foundation. Kathy Lu reports financial support was provided by the Air Force Office of Scientific Research.

## Data availability

Data will be made available on request.

## Appendix A. Supplementary data

Supplementary data to this article can be found online at https://doi.org/10.1016/j.matchemphys.2024.129123.

## References

- P. Colombo, G. Mera, R. Riedel, G.D. Sorarù, Polymer-derived ceramics: 40 years of research and innovation in advanced ceramics, J. Am. Ceram. Soc. 93 (7) (2010) 1805–1837.
- [2] R. Anand, S.P. Sahoo, B.B. Nayak, S.K. Behera, Phase evolution in Zr-doped preceramic polymer derived SiZrOC hybrids, Ceram. Int. 46 (7) (2020) 9962–9967.
- [3] M.A. Schiavon, C. Gervais, F. Babonneau, G.D. Soraru, Crystallization behavior of novel silicon boron oxycarbide glasses, J. Am. Ceram. Soc. 87 (2) (2004) 203–208.
- [4] E. Ionescu, H.-J. Kleebe, R. Riedel, Silicon-containing polymer-derived ceramic nanocomposites (PDC-NCs): preparative approaches and properties, Chem. Soc. Rev. 41 (15) (2012) 5032–5052.
- [5] J. Parmentier, G.D. Soraru, F. Babonneau, Influence of the microstructure on the high temperature behaviour of gel-derived SiOC glasses, J. Eur. Ceram. Soc. 21 (6) (2001) 817–824.

- [6] H.-J. Kleebe, C. Turquat, G.D. Sorarù, Phase separation in a SiCO glass studied by transmission electron microscopy and electron energy-loss spectroscopy, J. Am. Ceram. Soc. 84 (5) (2001) 1073–1080.
- [7] Q. Wen, Z. Yu, R. Riedel, The fate and role of in situ formed carbon in polymerderived ceramics, Prog. Mater. Sci. 109 (2020) 100623.
- [8] A.W. Weimer, K.J. Nilsen, G.A. Cochran, R.P. Roach, Kinetics of carbothermal reduction synthesis of beta silicon carbide, AIChE J. 39 (3) (1993) 493–503.
- [9] A.V. Rau, K. Knott, K. Lu, Porous SiOC/SiC ceramics via an active-filler-catalyzed polymer-derived method, Mater. Chem. Front. 5 (17) (2021) 6530–6545.
- [10] H. Chaney, K. Lu, New findings related to carbothermal reduction of polysiloxane-derived ceramics, Ceram. Int. 49 (6) (2023) 10193–10197.
- [11] A. Saha, R. Raj, Crystallization maps for SiCO amorphous ceramics, J. Am. Ceram. Soc. 90 (2) (2007) 578–583.
- [12] G. Gregori, H.-J. Kleebe, Y.D. Blum, F. Babonneau, Evolution of C-rich SiOC ceramics. Part II. Characterization by high lateral resolution techniques: electron energy-loss spectroscopy, high-resolution TEM and energy-filtered TEM 97 (6) (2006) 710–720
- [13] R. Anand, S.P. Sahoo, B.B. Nayak, S.K. Behera, Phase evolution, nanostructure, and oxidation resistance of polymer derived SiTiOC ceramic hybrid, Ceram. Int. 45 (5) (2019) 6570–6576.
- [14] L. Wang, K. Lu, R. Ma, Effects of different polymer precursors on the characteristics of SiOC bulk ceramics, Appl. Phys. A 125 (6) (2019) 395.
- [15] N. Yang, K. Lu, Porous and ultrahigh surface area SiOC ceramics based on perhydropolysilazane and polysiloxane, Microporous Mesoporous Mater. 306 (2020) 110477.
- [16] D. Erb, K. Lu, Synthesis of SiOC using solvent-modified polymer precursors, Mater. Chem. Phys. 237 (2019) 121844.
- [17] D. Erb, K. Lu, Effect of additive structure and size on SiO<sub>2</sub> formation in polymer-derived SiOC ceramics, J. Am. Ceram. Soc. 101 (12) (2018) 5378–5388.
- [18] D. Erb, K. Lu, Influence of vinyl bonds from PDMS on the pore structure of polymer derived ceramics, Mater. Chem. Phys. 209 (2018) 217–226.
- [19] D. Erb, K. Lu, Effects of SiO<sub>2</sub>-forming additive on polysiloxane derived SiOC ceramics, Microporous Mesoporous Mater. 266 (2018) 75–82.
- [20] H. Chaney, Y. Zhou, K. Lu, Understanding SiOC atomic structures via synchrotron X-ray and reactive force field potential studies, Mater. Today Chem. 29 (2023) 101429.
- [21] H. Chaney, K. Lu, ReaxFF simulation of pyrolysis behaviors of polysiloxane precursors with different carbon content, Chem. Mater. 35 (10) (2023) 3902–3910.
- [22] N. Yang, C. Ophus, B.H. Savitzky, M. Scott, K. Bustillo, K. Lu, Amorphous and crystalline co-existing SiOC phase analysis using 4D-STEM, Mater. Char. 181 (2021) 111512.
- [23] R. Pena-Alonso, G.D. Soraru, R. Raj, Preparation of ultrathin-walled carbon-based nanoporous structures by etching pseudo-amorphous silicon oxycarbide ceramics, J. Am. Ceram. Soc. 89 (8) (2006) 2473–2480.
- [24] B. Santhosh, E. Ionescu, F. Andreolli, M. Biesuz, A. Reitz, B. Albert, G.D. Sorarù, Effect of pyrolysis temperature on the microstructure and thermal conductivity of

- polymer-derived monolithic and porous SiC ceramics, J. Eur. Ceram. Soc. 41 (2) (2021) 1151–1162.
- [25] G.D. Sorarù, G. D'Andrea, R. Campostrini, F. Babonneau, G. Mariotto, Structural characterization and high-temperature behavior of silicon oxycarbide glasses prepared from sol-gel precursors containing Si-H bonds, J. Am. Ceram. Soc. 78 (2) (1995) 379–387.
- [26] T. Rouxel, G. Massouras, G.-D. Sorarù, High temperature behavior of a gelderived SiOC glass: elasticity and viscosity, J. Sol. Gel Sci. Technol. 14 (1) (1999) 87–94.
- [27] K. Bawane, D. Erb, K. Lu, Carbon content and pyrolysis atmosphere effects on phase development in SiOC systems, J. Eur. Ceram. Soc. 39 (9) (2019) 2846–2854.
- [28] G.J. Leonel, X. Guo, G. Singh, A. Navrotsky, Chemistry, structure, and thermodynamic stabilization of SiOC polymer derived ceramics made from commercial precursors, Open Ceramics 15 (2023) 100402.
- [29] A. Kaur, P. Chahal, T. Hogan, Selective fabrication of SiC/Si diodes by excimer laser under ambient conditions, IEEE Electron. Device Lett. 37 (2) (2016) 142–145.
- [30] A.H. Tavakoli, R. Campostrini, C. Gervais, F. Babonneau, J. Bill, G.D. Sorarù, A. Navrotsky, Energetics and structure of polymer-derived Si-(B-)O-C glasses: effect of the boron content and pyrolysis temperature, J. Am. Ceram. Soc. 97 (1) (2014) 303-309
- [31] M. Niu, H. Wang, J. Chen, L. Su, D. Wu, A. Navrotsky, Structure and energetics of SiOC and SiOC-modified carbon-bonded carbon fiber composites, J. Am. Ceram. Soc. 100 (8) (2017) 3693–3702.
- [32] T. Varga, A. Navrotsky, J.L. Moats, R.M. Morcos, F. Poli, K. Müller, A. Saha, R. Raj, Thermodynamically stable Si O C polymer-like amorphous ceramics, J. Am. Ceram. Soc. 90 (10) (2007) 3213-x3219.
- [33] H. Wang, W. Zhu, X. Sun, D. Su, Preparation of aerogel-like SiOC ceramic with honeycomb structure and its high-temperature performance, J. Alloys Compd. 937 (2023) 168438.
- [34] G. Mera, A. Navrotsky, S. Sen, H.-J. Kleebe, R. Riedel, Polymer-derived SiCN and SiOC ceramics structure and energetics at the nanoscale, J. Mater. Chem. A 1 (12) (2013) 3826–3836.
- [35] G.J. Leonel, X. Guo, G. Singh, A. Navrotsky, Compositional analysis of SiOC(H) powders: a comparison of X-ray Photoelectron Spectroscopy (XPS) and combustion analysis, Ceramics 6 (2023) 74–85.
- [36] A.H. Tavakoli, P. Gerstel, J.A. Golczewski, J. Bill, Effect of boron on the crystallization of amorphous Si–(B–)C–N polymer-derived ceramics, J. Non-Cryst. Solids 355 (48) (2009) 2381–2389.
- [37] A.H. Tavakoli, J.A. Golczewski, J. Bill, A. Navrotsky, Effect of boron on the thermodynamic stability of amorphous polymer-derived Si(B)CN ceramics, Acta Mater. 60 (11) (2012) 4514–4522.
- [38] N. Yang, K. Lu, Phase content prediction in polymer-derived ceramics with metal additives, J. Am. Ceram. Soc. 104 (10) (2021) 5379–5391.